



UNIVERSITY OF LEEDS

This is a repository copy of *Dynamic Crystallization Pathways of Polymorphic Pharmaceuticals Revealed in Segmented Flow with Inline Powder X-ray Diffraction*.

White Rose Research Online URL for this paper:
<https://eprints.whiterose.ac.uk/161413/>

Version: Accepted Version

Article:

Levenstein, MA orcid.org/0000-0002-2309-3743, Wayment, L, Scott, CD et al. (8 more authors) (2020) Dynamic Crystallization Pathways of Polymorphic Pharmaceuticals Revealed in Segmented Flow with Inline Powder X-ray Diffraction. *Analytical Chemistry*, 92 (11). pp. 7754-7761. ISSN 0003-2700

<https://doi.org/10.1021/acs.analchem.0c00860>

© 2020 American Chemical Society. This is an author produced version of an article published in *Analytical Chemistry*. Uploaded in accordance with the publisher's self-archiving policy.

Reuse

Items deposited in White Rose Research Online are protected by copyright, with all rights reserved unless indicated otherwise. They may be downloaded and/or printed for private study, or other acts as permitted by national copyright laws. The publisher or other rights holders may allow further reproduction and re-use of the full text version. This is indicated by the licence information on the White Rose Research Online record for the item.

Takedown

If you consider content in White Rose Research Online to be in breach of UK law, please notify us by emailing eprints@whiterose.ac.uk including the URL of the record and the reason for the withdrawal request.



eprints@whiterose.ac.uk
<https://eprints.whiterose.ac.uk/>

Dynamic Crystallization Pathways of Polymorphic Pharmaceuticals Revealed in Segmented Flow with Inline Powder XRD

Mark A. Levenstein,^{1, 2†#} Lois Wayment,^{3, 4, 5‡} C. Daniel Scott,^{3, 6} Ruth Lunt,^{3, 4} Pierre-Baptiste Flandrin,³ Sarah J. Day,⁵ Chiu C. Tang,⁵ Chick C. Wilson,³ Fiona C. Meldrum,² Nikil Kapur,¹ and Karen Robertson^{3†*}

¹ School of Mechanical Engineering, University of Leeds, Woodhouse Lane, Leeds LS2 9JT, UK, ² School of Chemistry, University of Leeds, Woodhouse Lane, Leeds LS2 9JT, UK, ³ Department of Chemistry, University of Bath, Claverton Down, Bath BA2 7AY, UK, ⁴ CMAC Future Manufacturing Hub, University of Bath, Claverton Down, Bath BA2 7AY, UK, ⁵ Diamond Light Source, Harwell Campus, Didcot, Oxfordshire OX11 0DE, UK, ⁶ Centre for Sustainable Chemical Technologies, University of Bath, Claverton Down, Bath BA2 7AY, UK, *email: Karen.Robertson@nottingham.ac.uk

ABSTRACT:

Understanding the transitions between polymorphs is essential in the development of strategies for manufacturing and maximizing the efficiency of pharmaceuticals. However, this can be extremely challenging: crystallization can be influenced by subtle changes in environment such as temperature and mixing intensity or even imperfections in the crystallizer walls. Here, we highlight the importance of *in situ* measurements in understanding crystallization mechanisms, where a segmented flow crystallizer was used to study the crystallization of the pharmaceuticals urea:barbituric acid (UBA) and carbamazepine (CBZ). The reactor provides highly reproducible reaction conditions, while *in situ* synchrotron powder X-ray diffraction (PXRD) enables us to monitor the evolution of this system. UBA has two polymorphs of almost equivalent free-energy and so is typically obtained as a polymorphic mixture. *In situ* PXRD uncovered a progression of polymorphs from UBA III to the thermodynamic polymorph UBA I, where different positions along the length of the tubular flow crystallizer correspond to different reaction times. Addition of UBA I seed crystals modified this pathway such that only UBA I was observed throughout, while transformation from UBA III into UBA I still occurred in the presence of UBA III seeds. Information regarding the mixing-dependent kinetics of the CBZ form II to III transformation was also uncovered in a series of seeded and unseeded flow crystallization runs, despite atypical habit expression. These results illustrate the importance of coupling controlled reaction environments with *in situ* XRD to study the phase relationships in polymorphic materials.

INTRODUCTION

The relative stabilities of polymorphic solid forms, the ability to selectively access individual polymorphs and the transitions between polymorphs, are all critical elements in the development and processing of solid-state pharmaceutical materials.^{1, 2} However, it can be difficult to predict crystallization routes and reproducibly select for a particular form, where post-crystallization analysis can only reveal limited information on the crystallization process itself and can be unreliable due to issues with quenching, drying, and sample preparation.³ In order to control the formation of such materials, an understanding of their real-time evolution in industrially-relevant environments is vital. X-ray diffraction (XRD) is a key analytical method for examining such systems, but examples of *in situ* diffraction studies are currently limited to small-scale batch and microfluidic reactors.

In order to better understand crystallization processes, more reproducible methods are required to control these processes over multiple length scales. Due to the inhomogeneity and irreproducibility of batch crystallizers, flow technologies have recently emerged as a highly effective means of achieving this goal.⁴ Continuous flow platforms that can simultaneously provide direct scale-out routes,⁵ narrow time resolution,⁶ representative sampling,⁷ and high-throughput materials synthesis up to production-scale rates are particularly attractive.⁸ Importantly, they can also be coupled to *in situ* analytical techniques. However, these technologies are still in their infancy, and few examples exist where flow platforms – especially large-scale platforms – have been used in conjunction with *in situ* analysis to evaluate crystallization pathways.⁹⁻¹³

Typically these have been limited to the production of sub-micron or nanoparticle-sized inorganic materials¹¹ or proteins,¹⁴ which present fewer challenges for blockage mitigation and back mixing. Additional *in situ* studies of crystallization processes have been conducted with smaller-scale microfluidic platforms using techniques such as optical microscopy¹⁵ and small angle X-ray scattering.^{16, 17} However, many time-resolved microfluidic studies have primarily focused on characterizing photoluminescent nanocrystals that can be monitored by fluorescence/absorption spectroscopy.¹⁸⁻²⁰ The few examples of millifluidic studies using *in situ* XRD either focus on crystallization events occurring on the reactor walls²¹ or divert the crystallizing solution into an add-on slurry cell which is not an integral part of the crystallizer.^{11, 22} For the latter case, this additional flow path can affect the crystallization environment and be prone to encrustation, and thus does not provide a representative expression of the crystallization pathway. Taddei and co-workers have demonstrated a millifluidic microwave-assisted flow crystallization apparatus which incorporates *in situ* powder XRD (PXRD) without a separate slurry cell.¹⁰ However, due to the constraints of this reactor

design, analysis is limited to a single location at the reactor outlet, preventing the investigation of reaction dynamics. These issues are addressed here, where we have successfully integrated a continuous millifluidic crystallizer with *in situ* synchrotron PXRD at multiple analysis points.

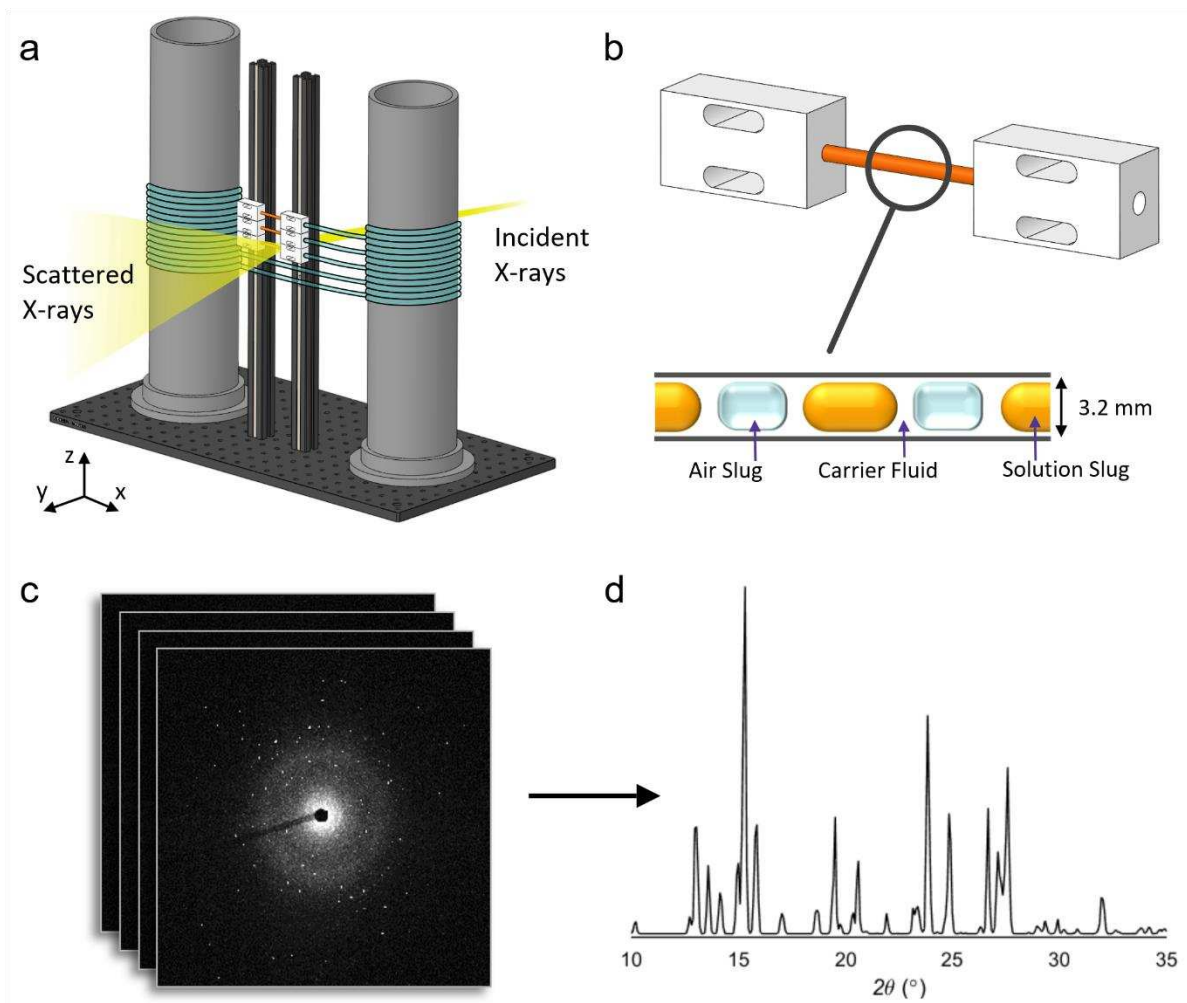


Figure 1: (a) Diagram of the analysis module of the KRAIC-D operating in transmission mode with X-ray penetration initiated behind the window section. (b) Enlarged view of a single analysis window comprising a Kapton tube and two polytetrafluoroethylene (PTFE) unions (inset shows the triphasic solution, air, and carrier fluid slug flow). (c) Accumulation of 2D diffraction pattern frames from 100 ms exposures that are combined to achieve a (d) 1D diffraction plot (shown here is a combined scan of carbamazepine form II).

We introduce the Kinetically Regulated Automated Input Crystallizer for Diffraction (KRAIC-D; Fig. 1), and demonstrate its use to study the crystallization pathways of two important polymorphic pharmaceutical model compounds: carbamazepine (CBZ) and urea:barbituric acid (UBA). The design of the KRAIC-D crystallizer is based upon the previously published KRAIC,^{13, 23-25} with a spatial rearrangement and inclusion of features such as X-ray transparent windows necessary for the implementation of *in situ* PXRD. X-ray diffraction provides critical structural information and, importantly, can be applied to all crystalline materials.

Additionally, our tri-segmented flow regime is shown to offer highly reproducible crystallization environments by limiting the influence of unwanted surfaces on crystallization, while the scale of the KRAIC-D allows for the analysis of large organic crystals (>100 μm) inaccessible with microfluidics.

An inherent property of segmented flow technologies is that, in steady flow, the residence or dwell time of particular fluid segments can be easily determined from their position along the flow path.²⁶ As such, analysis of a particular position within the flow will continually yield information from a single reaction time-point, irrespective of fluid motion or the transience of the process being studied. Thus, collecting diffraction data from a range of positions within a device enables step-by-step elucidation of dynamic crystallization pathways with excellent reproducibility. This concept has been successfully reported in a microfluidic system²⁷ and is adapted here at the milliliter-scale to uncover the crystallization pathways of CBZ and UBA in response to different seeding regimes. In addition to uncovering information regarding the mixing-dependent kinetics of the CBZ form II to III transformation, our results also provide clarity regarding the stability of UBA polymorphs under solvated or non-solvated conditions.

EXPERIMENTAL SECTION

Materials: Urea and barbituric acid were purchased from Sigma Aldrich (Steinheim, Germany) and carbamazepine was purchased from Molekula (Darlington, UK). All reagents were used without further purification. Laboratory grade solvents (methanol and ethanol) purchased from Sigma Aldrich were used for all crystallizations.

KRAIC-D Design and Operation: The KRAIC-D crystallizer consists of two modules: a control module containing fluid pumps and temperature control apparatus (Fig. S1) and an analysis module comprising the bulk of the flow reactor length and low scattering X-ray analysis windows (Fig. 1a). The analysis module was built from an optomechanical breadboard (Thorlabs) comprising two columns for coiling the reactor tubing and can be mounted onto the motorized stage of the beamline experimental hutch for beam positioning and data acquisition. Each analysis window is made from a seamless polyimide tube (Kapton, American Durafilm) that is integrated into the main fluorinated ethylene propylene (FEP, Omega) reactor tubing using custom-machined polytetrafluoroethylene (PTFE) unions (Fig. 1b and Fig. S4). Crystallizations were conducted in a tri-segmented flow of solvent, carrier fluid, and air to isolate reactions from the reactor walls and improve mixing and time-resolution (through minimization of Taylor dispersion²⁸). The air

phase aids in consistent flow segmentation and prevents coalescence of solution slugs in inclined sections of tubing. Cooling crystallizations of UBA and CBZ (from methanol and ethanol respectively) were studied unseeded and with the addition of slurries of seed crystals at two different seeding ports (see Supporting Information). Heated feed solutions were air-cooled to ambient temperature along the length of the crystallizer once segmentation was established, and seed slurries were prepared and added at room temperature.

In situ Powder XRD: Data were collected at the High-Resolution Powder Diffraction beamline (I11) of Diamond Light Source. Complete PXRD datasets were obtained through a serial crystallography-like approach, combining reflections from individual diffraction events caused by the flow of crystals past an X-ray beam.²⁹ In contrast to injector-based serial crystallography,^{30, 31} crystals are grown *in situ*, and different positions along the flow channel correspond to different times in the crystallization process.²⁷ Five separate multi-frame scans, each of 10.1 s total exposure time, from a single position along the flow are combined to produce a serial diffraction pattern for each time point (Fig. 1c). Each pattern is then azimuthally integrated and presented at the Cu K α characteristic wavelength (1.5406 Å) for comparison to reference data (Fig. 1d). Full experimental details, including detailed KRAIC-D designs and data capture and analysis procedures, are available in the Supporting Information.

RESULTS AND DISCUSSION

This study focused on the crystallization of two model pharmaceutical compounds – UBA and CBZ – to determine the relative stabilities of their different polymorphic forms, and the pathways by which they form. The co-crystalline system of UBA is a promising high solubility form of the barbiturate precursor, barbituric acid. Three atmospheric pressure polymorphs of UBA are known, where a mixture of UBA I and III is often obtained from cooling crystallization. Although some studies report contradicting results,^{32, 33} we have previously found UBA I to be the stable polymorph under normal cooling crystallization conditions.³⁴ However, the free energy levels of forms I and III are thought to be very close due to their concomitant production. UBA is therefore an ideal model for *in situ* XRD analysis.

CBZ is a high-profile pharmaceutical model molecule³⁵ and is the active pharmaceutical ingredient in Tegretol®, which is used as an anti-seizure medication and to relieve neuropathic pain. CBZ can crystallize in one of five polymorphs, of which CBZ III is the most stable under atmospheric pressure and CBZ II is

often the first to form during crystallization from solution.³⁶ A transformation between these two polymorphs can be expected during crystallization, whilst the initial polymorphic expression can be dependent on the mixing conditions.

UBA crystallization: UBA was crystallized in methanol under cooling in the absence and presence of UBA seed crystals in the KRAIC-D crystallizer. Initial offline PXRD analysis of unseeded material revealed a mixture of UBA I and III (Fig. S13), as has also been reported in previous studies.³⁴ This concomitant formation has led to some debate regarding the identity of the thermodynamic polymorph.³² During unseeded KRAIC-D experiments pure UBA III was observed at Window 1 (4.6 min, 6.4 m), but at Window 2 (6.9 min, 9.0 m) peaks of UBA I can clearly be seen, notably at $28.9^\circ 2\theta$ (3.08 \AA) corresponding to the $(11\bar{4})$ reflection (Fig. 2). Furthermore, the intensity of this UBA I peak with respect to UBA III peaks increases in the data obtained from Window 3 (9.0 min, 11.7 m). This suggests that UBA III is transforming into UBA I in solution with time and lends additional support to the identification of UBA III as the kinetic polymorph and UBA I as the thermodynamic polymorph.

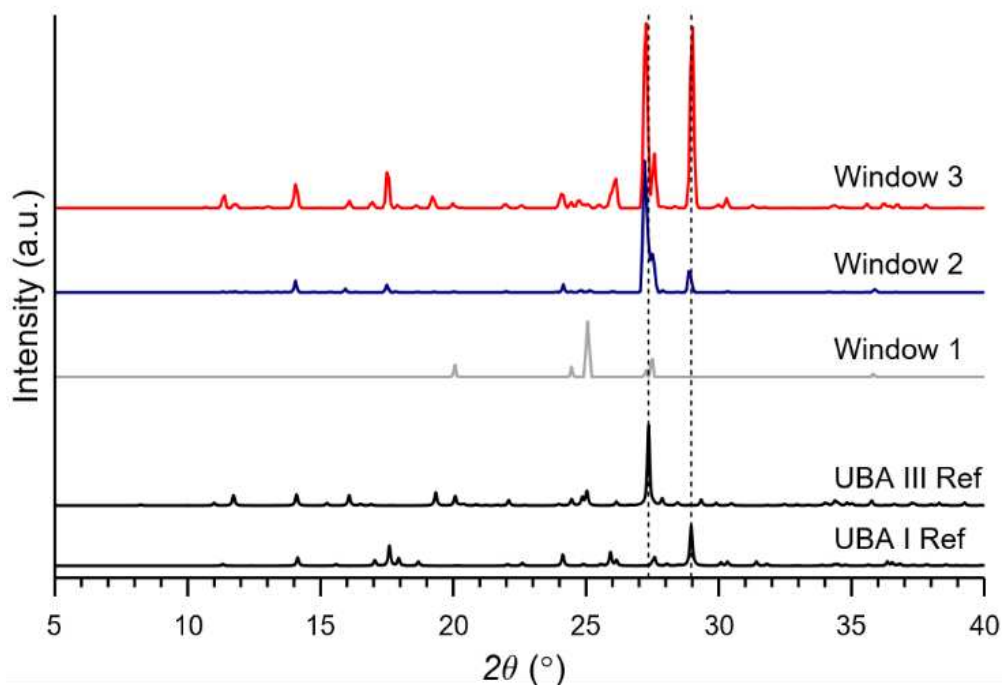


Figure 2: Unseeded cooling crystallization of UBA in the KRAIC-D showing a progression of form III to form I in PXRD patterns obtained from Window 1 to 3. The dotted lines are a guide to the eye for identification of characteristic peaks of each polymorph (UBA I and III). The scale of the experimental diffraction patterns has been adjusted for clarity and converted into Cu $K\alpha$ wavelength for comparison to reference data.

Experiments seeded with UBA I and UBA III crystals reinforce this interpretation. In experiments where seeds of UBA I were added at the onset of the reaction (immediately after segmentation is established, hereafter termed 'pre-nucleation', Fig. S5), only UBA I was observed along the entire crystallizer length (Fig. 3a and Fig. S14). Conversely, experiments with pre-nucleation seeding of UBA III again showed a slight conversion to UBA I by Window 2 (notably from peaks at 17.6 and 28.9°), confirming that UBA I is the thermodynamic form (Fig. 3a and Fig. S15). Furthermore, experiments seeded with UBA III at 9.1 m, after Window 2, (i.e. after where UBA I formed in the unseeded experiments, hereafter termed 'post-nucleation') still showed evidence of conversion of UBA III to I between Windows 2 and 3, notably through peaks at 17.6 and 28.9° (Fig. 3b).

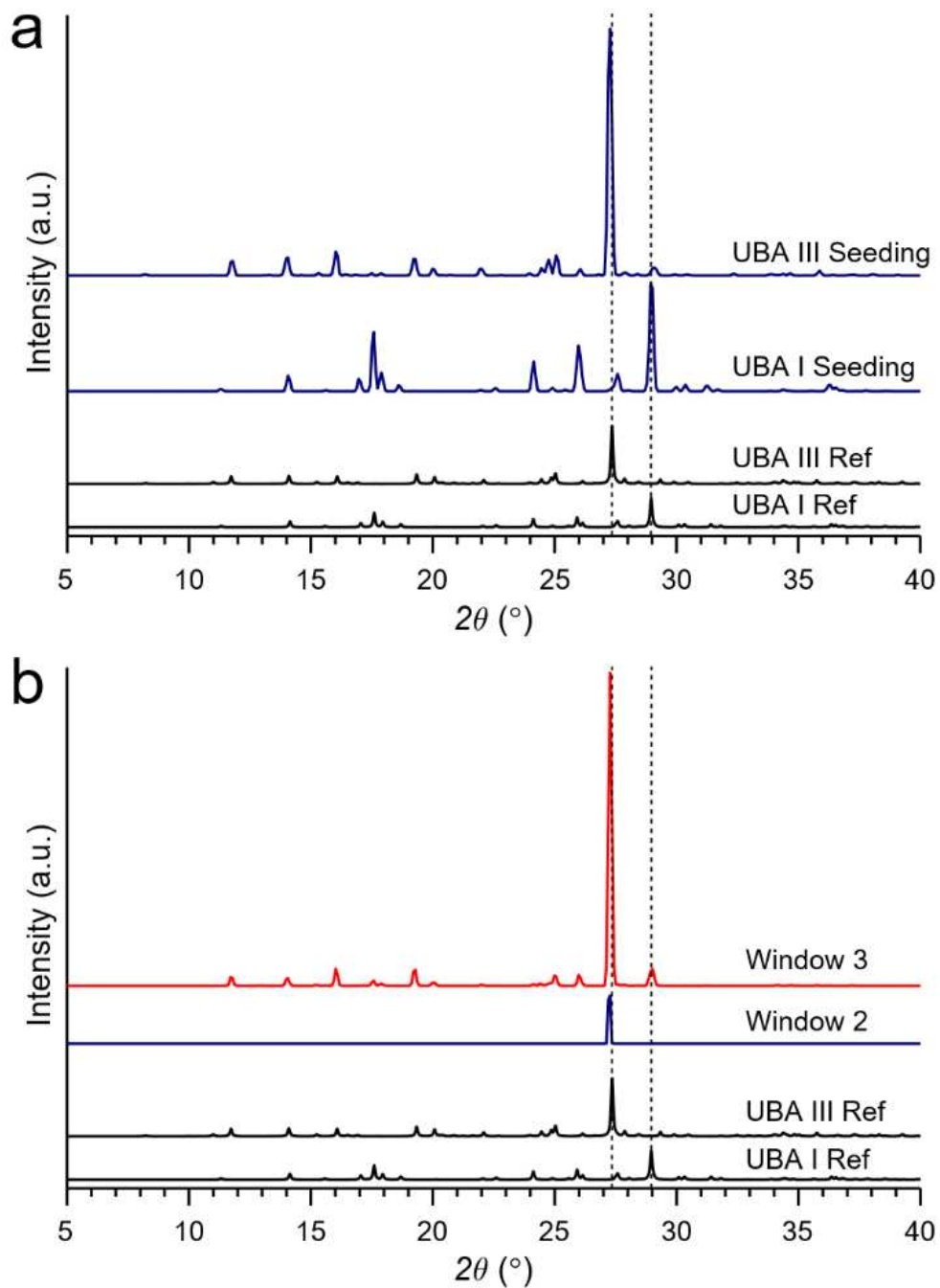


Figure 3: (a) PXR comparing UBA pre-nucleation seeded crystallization runs from Window 2. (b) PXR plots of UBA form III post-nucleation seeded run showing partial transformation to form I across Windows 2 and 3. The dotted lines are a guide to the eye for identification of characteristic peaks of each polymorph (UBA I and III). The scale of the experimental diffraction patterns has been adjusted for clarity and converted into Cu $K\alpha$ wavelength for comparison to reference data.

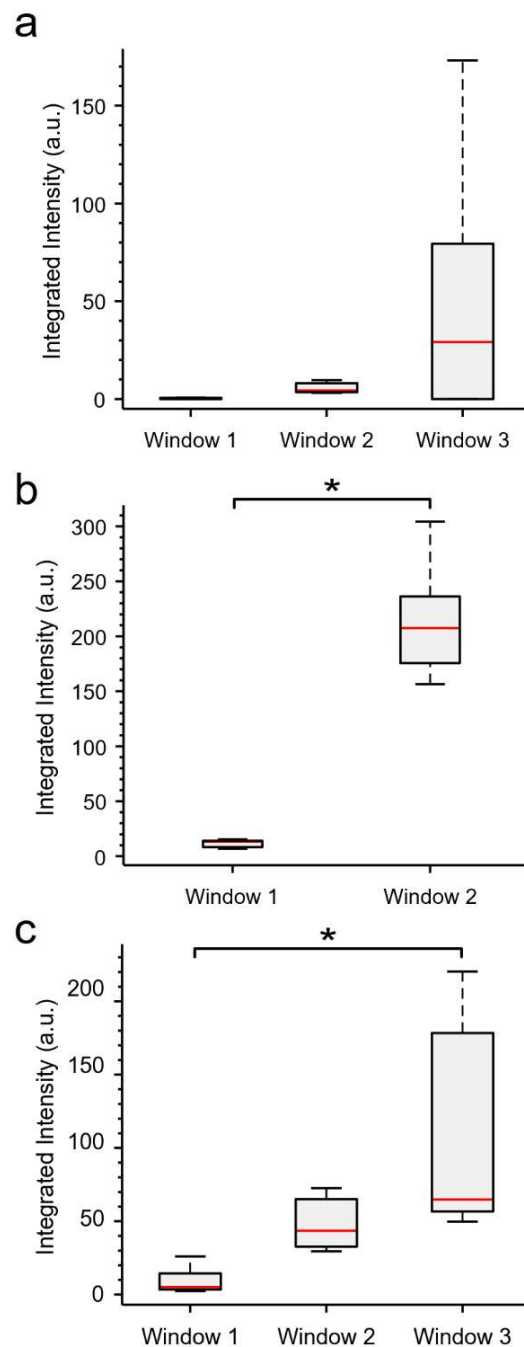


Figure 4: Box plots of diffraction intensity for (a) unseeded, (b) pre-nucleation form I seeded, and (c) pre-nucleation form III seeded UBA KRAIC-D experiments. N.B. red lines indicate the median intensity found in all frames containing non-solvent diffraction, boxes encompass the inner quartile range (*IQR*, between upper and lower quartiles), and data within $1.5 \times IQR$ are represented as whiskers. Asterisks indicate significant difference ($p < 0.05$).

Mapping crystal growth *via* relative diffraction intensity observed at each window (as defined by the area under the diffraction pattern or integrated intensity, see Supporting Information) shows that there is very little crystal growth between Windows 1 and 2 in the unseeded experiments (Fig. 4a). At Window 3 there is a large increase in diffraction intensity suggesting this system is nucleation limited with fast growth. In accordance with this, both experiments seeded pre-nucleation show significant growth between each window. Comparing the pre-nucleation seeded experiments, seeding with UBA I (Fig. 4b) produces a much greater increase in apparent crystal growth between window 1 and 2 than that observed for experiments seeded with UBA III (Fig. 4c). This could be attributed to the polymorphic conversion of UBA form III to I during the analyzed time period in UBA III seeded runs, not present when seeding with UBA form I.

In contrast to our *in situ* results, offline analysis of dry UBA I and III seeds after 12 months of storage at 18 °C in a standard laboratory environment showed some transformation of UBA I to UBA III, whilst UBA III seeds remained stable (Fig. S16). However, an additional offline experiment in which a slurry of these UBA III seeds was prepared in methanol for 4 mins again showed significant but incomplete transformation to UBA I (Fig S16, top). Previous literature reports have described the solid state transformation of UBA I to III^{32, 33, 37} and solution state transformation of UBA III to I.³⁴ In light of the findings reported here and the previous literature, we propose that the relative stability of the polymorph of UBA is dependent on environment, with UBA III being the most stable in air and UBA I being the most stable in solution.

CBZ crystallization: The crystallization of CBZ from ethanol with and without the addition of CBZ III seeds was studied in the KRAIC-D. In unseeded experiments, the metastable form, CBZ II, was observed throughout the crystallization process (observation points at 8 min 30 s, 12 min 20 s and 16 min 20 s, Fig. S17). Conversely, seeding the flow pre-nucleation with the thermodynamic form (CBZ III) resulted in the growth of exclusively CBZ III along the crystallizer length (Fig. S18). Further, when these same CBZ III seeds were added post-nucleation of CBZ II (at 12.7 min crystallization time, immediately after Window 2), all material appeared to have been converted to CBZ III by Window 3 (Fig. 5).

CBZ is well known to typically present morphologically as needles for CBZ II and as blocks for CBZ III. However, despite only detecting CBZ III by PXRD after post-nucleation seeding, aggregated needles were the main habit observed, in addition to a low proportion of small blocks and more plate-like crystals (video available in the Supporting Information). Additionally, offline slurring experiments of CBZ II and III seed

mixtures indicated there should be only a minor polymorphic transition (II \rightarrow III) within the timeframe between seeding at 12.7 min and detection at Window 3 (16.7 min; Fig. S19).

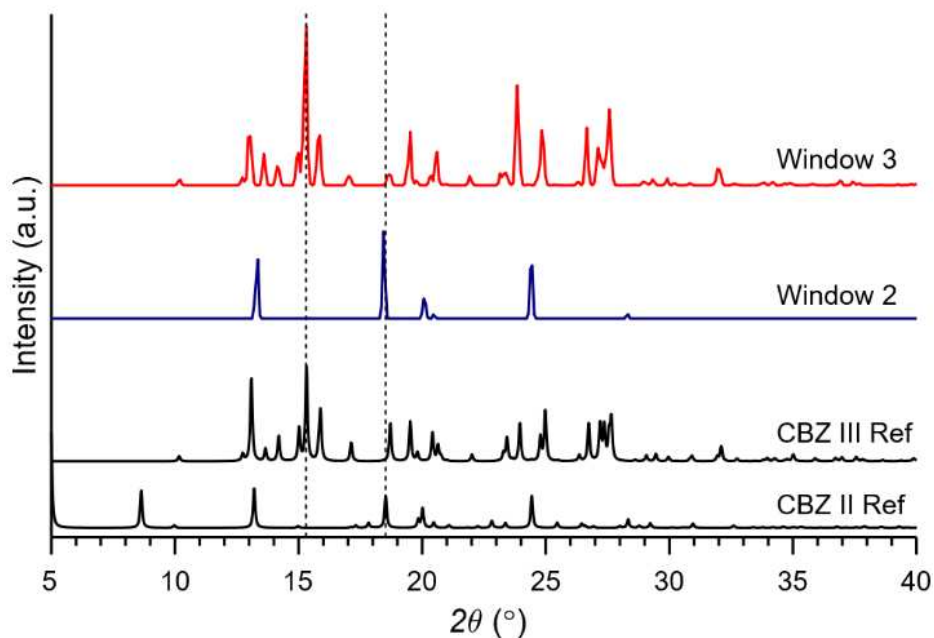


Figure 5: PXRD patterns obtained from CBZ cooling crystallization within the KRAIC-D with seeding of CBZ III post-nucleation (after Window 2). The dotted lines are a guide to the eye for identification of characteristic peaks of each polymorph (CBZ II and III). The scale of the experimental diffraction patterns has been adjusted for clarity and converted into Cu K α wavelength for comparison to reference data.

To test whether the diffraction of the more abundant needle crystals was obscured by the more naturally intensely diffracting prisms through combining diffraction patterns (comprising 255 individual frames), we analyzed individual 100 ms diffraction frames from both before and after the addition of CBZ III seeds (Fig. 6). At Window 2, prior to the addition of CBZ III seeds, diffraction peaks captured at 13.2°, 18.5°, and 24.4° corresponding to the (140)/(410), (211), and (431) reflections of CBZ II enabled its detection from a single frame (Fig. 6a). Subsequently, the combination of successive frames and scans confirmed the identification of CBZ II, with increased diffraction statistics of these peaks and the detection of additional reflections. However, at Window 3, even analysis of individual frames did not reveal any reflections that could have been produced by CBZ II crystals (Fig. 6b). Multiple diffraction peaks unique to CBZ III were observed in individual frames, notably at 15.3° and 19.5° corresponding to the (110) and (11 $\bar{3}$) reflections. Subsequent combination of frames/scans yielded new reflections consistent with the presence of CBZ III,

improving the agreement of relative peak heights with reference data. Therefore, due to only CBZ III being observed *via* PXRD and the high percentage of needles observed visually, we conclude that this must be a rare case of CBZ III presenting as needle crystals as was previously reported from cooling crystallization in isopropanol³⁸ or in the presence of surfactants.³⁹ Additionally, we rationalize the faster conversion of CBZ II to CBZ III observed in the KRAIC-D compared to batch slurring techniques by the intensified mixing induced within the segmented flow environment.⁴⁰

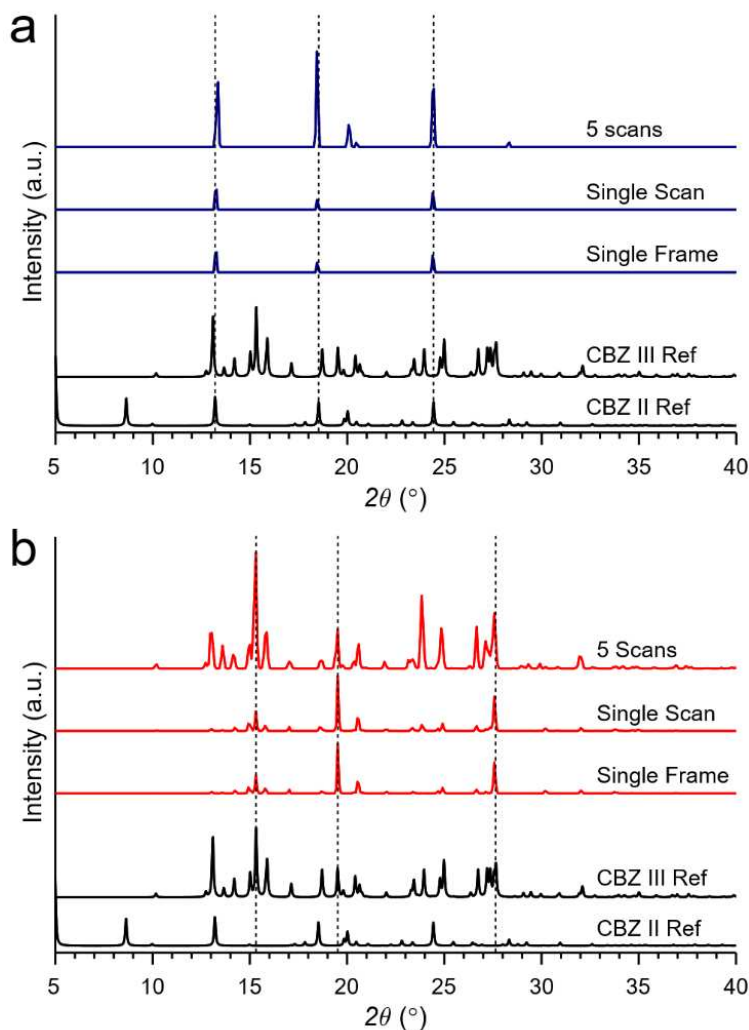


Figure 6: PXRD patterns of CBZ obtained from post-nucleation seeded cooling crystallization in the KRAIC-D at (a) Window 2 and (b) Window 3, comparing the data obtained from the combined scan method (5 scans), a single scan with a total of 51 exposures and a singular 100 ms exposure (frame). The dotted lines are a guide to the eye for the identification of selected characteristic peaks of CBZ II and III in (a) and (b), respectively. The scale of the experimental diffraction patterns has been adjusted for clarity and converted into Cu K α wavelength for comparison to reference data.

The growth profile of unseeded CBZ crystallization shows a significant exponential increase in relative diffraction intensity across the three analysis windows (Fig. 7a). Pre-nucleation seeded crystallization with CBZ III, however, achieves steady-state intensity prior to Window 1 (Fig. 7b), implying thermodynamic equilibrium has occurred before our first point of analysis (8 min 30 s). This is in contrast to the latent growth observed for unseeded UBA and linear growth profiles for pre-nucleation seeded crystallization with either UBA I or III.

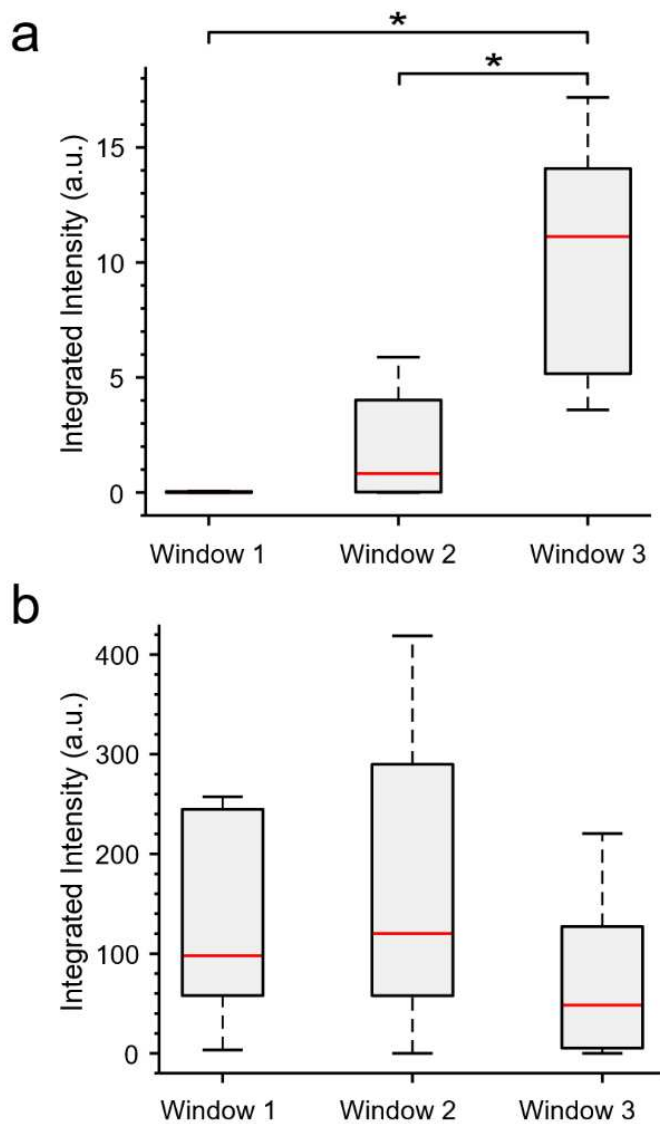


Figure 7: Box plots of diffraction intensity for (a) unseeded and (b) pre-nucleation form III seeded CBZ KRAIC-D experiments. N.B. red lines indicate the median intensity found in all frames containing non-solvent diffraction, boxes encompass the inner quartile range (*IQR*, between upper and lower quartiles), and data within $1.5 \times IQR$ are represented as whiskers. Asterisks indicate significant difference ($p < 0.05$).

CONCLUSIONS

Polymorphic transitions and stability during cooling crystallization in an industrially relevant crystallizer were uncovered through *in situ* powder X-ray diffraction (PXRD) analysis. The relationship between crystallizer length and reaction time in the milli-scale tubular crystallizer (KRAIC-D) provided reliable and reproducible access to transient crystallization events at the required time resolution. With this platform, we studied the crystallization pathways of two important pharmaceutical systems, urea:barbituric acid (UBA) and carbamazepine (CBZ), and assessed their polymorphism during unassisted crystallization and in response to various seeding regimes. For UBA, these experiments helped determine the relative stability of polymorphs in solution vs the solid state. During solution-based crystallization and slurring, UBA III rapidly transforms into UBA I in the presence and absence of seed crystals. In contrast, dry crystals of UBA I transform into UBA III under normal laboratory conditions within 12 months, highlighting the need for accurate knowledge of the media-dependent stability (in this case methanol vs air) of a solid form as essential for designing routes to accessing effective pharmaceuticals.

Experiments with CBZ confirmed the established form II to form III nucleation and growth pathway and illustrated the sensitivity of this pathway to seeding and mixing intensity. Nucleation of CBZ form II could be bypassed completely or existent form II crystals begin rapid transformation depending on the location of form III seeding. From a technical standpoint, deeper evaluation of CBZ data also showed that a single 100 ms diffraction frame from the KRAIC-D can yield sufficient data to identify polymorph.

The KRAIC-D complements previously reported examples of inline PXRD analysis^{10, 11, 21, 22} through direct inclusion of multiple non-invasive analysis windows with low background scattering. This new method also builds on our earlier work in microfluidic PXRD.²⁷ While microfluidic devices have a much smaller footprint in the beamline experimental hutch and can be more easily incorporated with additional analysis windows/ residence time points, they also are more prone to fouling and blockage from large crystals or in rapid precipitation scenarios than their milli-scale counterparts. Furthermore, the larger channel cross-section and slower relative speed of millifluidic flows are not as demanding of beamline hardware (i.e. do not require microfocused X-ray beams or <100 ms exposures), and thus lower the barrier to performing *in situ* structural analysis of target materials. We envisage this technique will enable new research into understanding and ultimately controlling crystallization processes. In particular, the ability to apply this strategy to large-scale crystallizers will facilitate expedited production and quality assurance of pharmaceuticals and agrochemicals in manufacturing environments.

ASSOCIATED CONTENT

Supporting Information

Detailed information regarding the experimental set-up, methodology and supporting experimental results is supplied as a word document, and a video showing the unusual needle habit of CBZ form III is supplied as a mp4 file in the supporting information. This material is available free of charge *via* the Internet at <http://pubs.acs.org>

AUTHOR INFORMATION

Corresponding Author

* Karen.Robertson@nottingham.ac.uk

Present Addresses

Present Address: Department of Mechanical Science and Engineering, University of Illinois at Urbana-Champaign, 1206 West Green Street, Urbana, Illinois 61801, United States

† Present Address: Department of Chemical and Environmental Engineering, University of Nottingham, University Park, Nottingham NG7 2RD

Author Contributions

‡These authors contributed equally

ACKNOWLEDGMENT

The authors would like to thank Vapourtec UK for the loan of a SF-10 low pulsation peristaltic pump for use as a seed solution delivery pump. We also acknowledge Diamond Light Source for awarding beamtime under proposals EE14807 and EE18771 and commissioning time NT18405-1. From Bath we would like to thank the UK Engineering and Physical Sciences Research Council (EPSRC) Future Continuous Manufacturing and Advanced Crystallization Research Hub (EP/P006965/1, Wilson, Wayment, Lunt), Diamond Light Source (Wayment), EPSRC Metastable Materials (EP/K004956/1, Flandrin) and the EPSRC Centre for Doctoral Training in Sustainable Chemical Technologies (EP/L016354/1, Scott) for funding. We acknowledge additional funding at Leeds from the EPSRC Platform Grant (EP/N002423/1) and the European Research Council (ERC) under the project DYNAMIN (DLV-788968). Levenstein acknowledges support from the Leeds International Research Scholarship. The authors additionally thank Graham Brown and Darren Harrison at the University of Leeds for machining the PTFE tubing unions. Levenstein would like to dedicate this article

to his grandmother, Rachelle Dube, who passed away unexpectedly the week prior to the original date of submission.

REFERENCES

- (1) Cox, J. R.; Ferris, L. A.; Thalladi, V. R., Selective growth of a stable drug polymorph by suppressing the nucleation of corresponding metastable polymorphs. *Angew. Chem. Int. Ed.*, **2007**, *46* (23), 4333-4336.
- (2) Sear, R. P., The non-classical nucleation of crystals: microscopic mechanisms and applications to molecular crystals, ice and calcium carbonate. *Int. Mater. Rev.*, **2012**, *57* (6), 328-356.
- (3) von Raumer, M.; Hilfiker, R., *Polymorphism in the Pharmaceutical Industry: Solid Form and Drug Development*. John Wiley & Sons: 2019; p 392.
- (4) Jiang, M.; Braatz, R. D., Designs of continuous-flow pharmaceutical crystallizers: developments and practice. *Crystengcomm* **2019**, *21* (23), 3534-3551.
- (5) Wang, T.; Lu, H. J.; Wang, J. K.; Xiao, Y.; Zhou, Y. A.; Bao, Y.; Hao, H. X., Recent progress of continuous crystallization. *J. Ind Eng Chem*, **2017**, *54*, 14-29.
- (6) Graceffa, R.; Nobrega, R. P.; Barrea, R. A.; Kathuria, S. V.; Chakravarthy, S.; Bilsel, O.; Irving, T. C., Sub-millisecond time-resolved SAXS using a continuous-flow mixer and X-ray microbeam. *J. Synchrotron Radiat* **2013**, *20*, 820-825.
- (7) Saldanha, O.; Graceffa, R.; Hemonnot, C. Y. J.; Ranke, C.; Brehm, G.; Liebi, M.; Marmioli, B.; Weinhausen, B.; Burghammer, M.; Koster, S., Rapid Acquisition of X-Ray Scattering Data from Droplet-Encapsulated Protein Systems. *Chemphyschem* **2017**, *18* (10), 1220-1223.
- (8) McGlone, T.; Briggs, N. E. B.; Clark, C. A.; Brown, C. J.; Sefcik, J.; Florence, A. J., Oscillatory Flow Reactors (OFRs) for Continuous Manufacturing and Crystallization. *Org Proc Res Dev* **2015**, *19* (9), 1186-1202.
- (9) Gerard, C. J. J.; Ferry, G.; Vuillard, L. M.; Boutin, J. A.; Chavas, L. M. G.; Huet, T.; Ferte, N.; Grossier, R.; Candoni, N.; Veessler, S., Crystallization via tubing microfluidics permits both in situ and ex situ X-ray diffraction. *Acta Crystallogr F*, **2017**, *73*, 574-578.
- (10) Taddei, M.; Casati, N.; Steitz, D. A.; Dumbgen, K. C.; van Bokhoven, J. A.; Ranocchiari, M., In situ high-resolution powder X-ray diffraction study of UiO-66 under synthesis conditions in a continuous-flow microwave reactor. *Crystengcomm* **2017**, *19* (23), 3206-3214.

- (11) Hammond, R. B.; Lai, X. J.; Roberts, K. J.; Thomas, A.; White, G., Application of in-process X-ray powder diffraction for the identification of polymorphic forms during batch crystallization reactions. *Cryst Growth Des*, **2004**, *4* (5), 943-948.
- (12) Sun, P. P.; Gjorup, F. H.; Ahlburg, J. V.; Mamakhel, A.; Wang, S. Z.; Christensen, M., In Situ In-House Powder X-ray Diffraction Study of Zero-Valent Copper Formation in Supercritical Methanol. *Cryst Growth Des* **2019**, *19* (4), 2219-2227.
- (13) Pallipurath, A. R.; Flandrin, P. B.; Wayment, L. E.; Wilson, C. C.; Robertson, K., In situ non-invasive Raman spectroscopic characterisation of succinic acid polymorphism during segmented flow crystallisation. *Mol Syst Des Eng* **2020**, *5* (1), 294-303.
- (14) Sui, S.; Perry, S. L., Microfluidics: From crystallization to serial time-resolved crystallography. *Struct Dyn* **2017**, *4* (3), 032202.
- (15) Zhang, S.; Ferte, N.; Candoni, N.; Veessler, S., Versatile Microfluidic Approach to Crystallization. *Org Proc Res Dev* **2015**, *19* (12), 1837-1841.
- (16) Alison, H. G.; Davey, R. J.; Garside, J.; Quayle, M. J.; Tiddy, G. J. T.; Clarke, D. T.; Jones, G. R., Using a novel plug flow reactor for the in situ, simultaneous, monitoring of SAXS and WAXD during crystallisation from solution. *Phys Chem Chem Phys* **2003**, *5* (22), 4998-5000.
- (17) Stehle, R.; Goerigk, G.; Wallacher, D.; Ballauff, M.; Seiffert, S., Small-angle X-ray scattering in droplet-based microfluidics. *Lab Chip* **2013**, *13* (8), 1529-1537.
- (18) Phillips, T. W.; Lignos, I. G.; Maceiczkyk, R. M.; deMello, A. J.; deMello, J. C., Nanocrystal synthesis in microfluidic reactors: where next? *Lab Chip* **2014**, *14* (17), 3172-3180.
- (19) Lignos, I.; Stavarakis, S.; Kilaj, A.; deMello, A. J., Millisecond-Timescale Monitoring of PbS Nanoparticle Nucleation and Growth Using Droplet-Based Microfluidics. *Small* **2015**, *11* (32), 4009-4017.
- (20) Epps, R. W.; Felton, K. C.; Coley, C. W.; Abolhasani, M., Automated microfluidic platform for systematic studies of colloidal perovskite nanocrystals: towards continuous nano-manufacturing. *Lab Chip* **2017**, *17* (23), 4040-4047.
- (21) Burkle, D.; De Motte, R.; Taleb, W.; Kleppe, A.; Comyn, T.; Vargas, S. M.; Neville, A.; Barker, R., Development of an electrochemically integrated SR-GIXRD flow cell to study FeCO₃ formation kinetics. *Rev Sci* **2016**, *87* (10).
- (22) Zhu, B., In Situ Analysis of Lactose Crystal in Solution through Slurry Flow Cell X-Ray Diffraction. *Cryst Res Technol* **2020**, *55* (4).
- (23) Robertson, K.; Flandrin, P.-B.; Klapwijk, A. R.; Wilson, C. C., Design and Evaluation of a Mesoscale Segmented Flow Reactor (KRAIC). *Cryst Growth Des* **2016**, *16*, 4759-4764.

- (24) Robertson, K.; Flandrin, P. B.; Shepherd, H. J.; Wilson, C. C., (Fe(Htrz)₂(trz)) (BF₄) nanoparticle production in a milli-scale segmented flow crystalliser. *Chem Today* **2017**, *35* (1), 19-22.
- (25) Scott, C. D.; Labes, R.; Depardieu, M.; Battilocchio, C.; Davidson, M. G.; Ley, S. V.; Wilson, C. C.; Robertson, K., Integrated plug flow synthesis and crystallisation of pyrazinamide. *React Chem Eng* **2018**, *3* (5), 631-634.
- (26) Song, H.; Chen, D. L.; Ismagilov, R. F., Reactions in droplets in microfluidic channels. *Angew Chem Int Ed* **2006**, *45* (44), 7336-7356.
- (27) Levenstein, M. A.; Anduix-Canto, C.; Kim, Y. Y.; Holden, M. A.; Nino, C. G.; Green, D. C.; Foster, S. E.; Kulak, A. N.; Govada, L.; Chayen, N. E.; Day, S.; Tang, C. C.; Weinhausen, B.; Burghammer, M.; Kapur, N.; Meldrum, F. C., Droplet Microfluidics XRD Identifies Effective Nucleating Agents for Calcium Carbonate. *Adv Funct Mater* **2019**, *29* (19), 1808172.
- (28) Cabeza, V. S.; Kuhn, S.; Kulkarni, A. A.; Jensen, K. F., Size-Controlled Flow Synthesis of Gold Nanoparticles Using a Segmented Flow Microfluidic Platform. *Langmuir* **2012**, *28* (17), 7007-7013.
- (29) Chapman, H. N.; Fromme, P.; Barty, A.; White, T. A.; Kirian, R. A.; Aquila, A.; Hunter, M. S.; Schulz, J.; DePonte, D. P.; Weierstall, U.; Doak, R. B.; Maia, F.; Martin, A. V.; Schlichting, I.; Lomb, L.; Coppola, N.; Shoeman, R. L.; Epp, S. W.; Hartmann, R.; Rolles, D.; Rudenko, A.; Foucar, L.; Kimmel, N.; Weidenspointner, G.; Holl, P.; Liang, M. N.; Barthelmess, M.; Caleman, C.; Boutet, S.; Bogan, M. J.; Krzywinski, J.; Bostedt, C.; Bajt, S.; Gumprecht, L.; Rudek, B.; Erk, B.; Schmidt, C.; Homke, A.; Reich, C.; Pietschner, D.; Struder, L.; Hauser, G.; Gorke, H.; Ullrich, J.; Herrmann, S.; Schaller, G.; Schopper, F.; Soltau, H.; Kuhn, K. U.; Messerschmidt, M.; Bozek, J. D.; Hau-Riege, S. P.; Frank, M.; Hampton, C. Y.; Sierra, R. G.; Starodub, D.; Williams, G. J.; Hajdu, J.; Timneanu, N.; Seibert, M. M.; Andreasson, J.; Rocker, A.; Jonsson, O.; Svenda, M.; Stern, S.; Nass, K.; Andritschke, R.; Schroter, C. D.; Krasniqi, F.; Bott, M.; Schmidt, K. E.; Wang, X. Y.; Grotjohann, I.; Holton, J. M.; Barends, T. R. M.; Neutze, R.; Marchesini, S.; Fromme, R.; Schorb, S.; Rupp, D.; Adolph, M.; Gorkhover, T.; Andersson, I.; Hirsemann, H.; Potdevin, G.; Graafsma, H.; Nilsson, B.; Spence, J. C. H., Femtosecond X-ray protein nanocrystallography. *Nature* **2011**, *470* (7332), 73-U81.
- (30) Nogly, P.; James, D.; Wang, D. J.; White, T. A.; Zatsepin, N.; Shilova, A.; Nelson, G.; Liu, H. G.; Johansson, L.; Heymann, M.; Jaeger, K.; Metz, M.; Wickstrand, C.; Wu, W. T.; Bath, P.; Berntsen, P.; Oberthuer, D.; Panneels, V.; Cherezov, V.; Chapman, H.; Schertler, G.; Neutze, R.; Spence, J.; Moraes, I.; Burghammer, M.; Standfuss, J.; Weierstall, U., Lipidic cubic phase serial millisecond crystallography using synchrotron radiation. *IUCrJ* **2015**, *2*, 168-176.

- (31) Wiedorn, M. O.; Oberthur, D.; Bean, R.; Schubert, R.; Werner, N.; Abbey, B.; Aepfelbacher, M.; Adriano, L.; Allahgholi, A.; Al-Qudami, N.; Andreasson, J.; Aplin, S.; Awel, S.; Ayyer, K.; Bajt, S.; Barak, I.; Bari, S.; Bielecki, J.; Botha, S.; Boukhelef, D.; Brehm, W.; Brockhauser, S.; Cheviakov, I.; Coleman, M. A.; Cruz-Mazo, F.; Danilevski, C.; Darmanin, C.; Doak, R. B.; Domaracky, M.; Dorner, K.; Du, Y.; Fangohr, H.; Fleckenstein, H.; Frank, M.; Fromme, P.; Ganán-Calvo, A. M.; Gevorkov, Y.; Giewekemeyer, K.; Ginn, H. M.; Graafsma, H.; Graceffa, R.; Greiffenberg, D.; Gumprecht, L.; Gottlicher, P.; Hajdu, J.; Hauf, S.; Heymann, M.; Holmes, S.; Horke, D. A.; Hunter, M. S.; Imlau, S.; Kaukher, A.; Kim, Y.; Klyuev, A.; Knoska, J.; Kobe, B.; Kuhn, M.; Kupitz, C.; Kuper, J.; Lahey-Rudolph, J. M.; Laurus, T.; Le Cong, K.; Letrun, R.; Xavier, P. L.; Maia, L.; Maia, F.; Mariani, V.; Messerschmidt, M.; Metz, M.; Mezza, D.; Michelat, T.; Mills, G.; Monteiro, D. C. F.; Morgan, A.; Muhlig, K.; Munke, A.; Munnich, A.; Nette, J.; Nugent, K. A.; Nuguid, T.; Orville, A. M.; Pandey, S.; Pena, G.; Villanueva-Perez, P.; Poehlsen, J.; Previtali, G.; Redecke, L.; Riekehr, W. M.; Rohde, H.; Round, A.; Safenreiter, T.; Sarrou, I.; Sato, T.; Schmidt, M.; Schmitt, B.; Schonherr, R.; Schulz, J.; Sellberg, J. A.; Seibert, M. M.; Seuring, C.; Shelby, M. L.; Shoeman, R. L.; Sikorski, M.; Silenzi, A.; Stan, C. A.; Shi, X. T.; Stern, S.; Sztuk-Dambietz, J.; Szuba, J.; Tolstikova, A.; Trebbin, M.; Trunk, U.; Vagovic, P.; Ve, T.; Weinhausen, B.; White, T. A.; Wrona, K.; Xu, C.; Yefanov, O.; Zatsepin, N.; Zhang, J. G.; Perbandt, M.; Mancuso, A. P.; Betzel, C.; Chapman, H.; Barty, A., Megahertz serial crystallography. *Nature Comm* **2018**, *9*, 4025.
- (32) Gryl, M.; Krawczuk, A.; Stadnicka, K., Polymorphism of urea-barbituric acid co-crystals. *Acta Crystallogr B* **2008**, *64*, 623-632.
- (33) Gryl, M.; Krawczuk-Pantula, A.; Stadnicka, K., Charge-density analysis in polymorphs of urea-barbituric acid co-crystals. *Acta Crystallogr B* **2011**, *67*, 144-154.
- (34) Powell, K. A.; Bartolini, G.; Wittering, K. E.; Saleemi, A. N.; Wilson, C. C.; Rielly, C. D.; Nagy, Z. K., Toward Continuous Crystallization of Urea-Barbituric Acid: A Polymorphic Co-Crystal System. *Cryst Growth Des* **2015**, *15* (10), 4821-4836.
- (35) Yang, H. Y.; Song, C. L.; Lim, Y. X. S.; Chen, W. Q.; Heng, J. Y. Y., Selective crystallisation of carbamazepine polymorphs on surfaces with differing properties. *Crystengcomm* **2017**, *19* (44), 6573-6578.
- (36) Sypek, K.; Burns, I. S.; Florence, A. J.; Sefcik, J., In Situ Monitoring of Stirring Effects on Polymorphic Transformations during Cooling Crystallization of Carbamazepine. *Cryst Growth Des* **2012**, *12* (10), 4821-4828.
- (37) Lunt, R. *University of Bath*, **2019**.
- (38) Nievergelt, P. P.; Spingler, B., Growing single crystals of small molecules by thermal recrystallization, a viable option even for minute amounts of material? *Crystengcomm* **2017**, *19* (1), 142-147.

(39) Nair, R.; Gonen, S.; Hoag, S. W., Influence of polyethylene glycol and povidone on the polymorphic transformation and solubility of carbamazepine. *Int J Pharm* **2002**, *240* (1-2), 11-22.

(40) Romano, M.; Pradere, C.; Sarrazin, F.; Toutain, J.; Batsale, J. C., Enthalpy, kinetics and mixing characterization in droplet-flow millifluidic device by infrared thermography. *Chem Eng J* **2015**, *273*, 325-332.

